Photoacoustic image reconstruction based on Bayesian compressive sensing algorithm

Mingjian Sun (孙明健)*, **Naizhang Feng (冯乃章)**, **Yi Shen (沈 毅)**, **Jiangang Li (李建刚)**,
Liyong Ma (马立勇), **and Zhenghua Wu (伍政华)**

Department of Control Science and Engineering, Harbin Institute of Technology, Harbin 150001, China
*Corresponding author: sunmingjian@hit.edu.cn

The photoacoustic tomography (PAT) method, based on compressive sensing (CS) theory, requires that, for the CS reconstruction, the desired image should have a sparse representation in a known transform domain. However, the sparsity of photoacoustic signals is destroyed because noises always exist. Therefore, the original sparse signal cannot be effectively recovered using the general reconstruction algorithm. In this study, Bayesian compressive sensing (BCS) is employed to obtain highly sparse representations of photoacoustic images based on a set of noisy CS measurements. Results of simulation demonstrate that the BCS-reconstructed image can achieve superior performance than other state-of-the-art CS-reconstruction algorithms.

OCIS codes: 100.3020, 110.5120, 170.5120.
doi: 10.3788/COL201109.061002.

Photoacoustic imaging, in recent times, has emerged as a promising imaging technique for biomedical applications[1]. Several physiologically important molecules, such as hemoglobin, possess a high characteristic absorption; therefore, photoacoustic imaging provides superlative quality images of vasculature and hemodynamic functions *in vivo*[2−5]. In photoacoustic imaging, a pulsed broad laser beam illuminates the biological tissue to generate a rapid increase in temperature. The resultant thermoelastic expansion leads to the emission of short-wavelength pulsed ultrasonic waves. These acoustic waves are detected by ultrasonic transducers, and an image is then reconstructed from signals recorded at different locations surrounding the tissue.

In photoacoustic tomography (PAT) imaging, the reconstruction algorithms existing for circular tomography require a great number of measurements, which require complex and expensive electronic equipments. In addition, it is almost impossible to cover the entire surface of tissue in practice; therefore, the data can often be acquired from limited view angles. To resolve such limiting factors, Provost *et al.* demonstrated that the theory of compressive sensing (CS) can be used for reconstruction in PAT by using a small number of angles[6]. Liang *et al.* applied the CS theory to address the issue of artifacts in limited-view imaging and to reduce the number of random illuminations for fast data-acquisition[7]. Guo *et al.* incorporated the CS theory in the PAT reconstruction. Both phantom and *in vivo* results showed that the CS method can effectively reduce the number of undersampling artifacts[8].

Nonetheless, in practice, photoacoustic signals are often polluted by noises[9]. Noisy signals are not strictly sparse signals, but they are compressible signals. In the abovementioned CS-based PAT theory, basis functions that are once added are never removed. A successful application of CS requires that the desired image must have a sparse representation in a known transform domain; however, the noise destroys the sparsity of photoacoustic signals. In such noisy conditions, the original sparse signal cannot be effectively recovered.

In this letter, a Bayesian compressive sensing (BCS) method is employed to obtain highly sparse representations of photoacoustic images based on a set of noisy CS measurements. It has been demonstrated, in the sparse Bayesian learning literature, that utilization of the relevance vector machine (RVM)[10] can facilitate more effective resolution of problems in CS[11].

Based on the CS method, if a given image f is compressible in a transform basis function Ψ, it is possible to perform a compressed set of measurements y: in case of CS measurements corrupted by an approximated zero-mean Gaussian noise n with unknown variance σ^2, CS measurements may be represented as

$$y = \Phi\omega + n, \tag{1}$$

where $\Phi = [\varphi_1, \cdots, \varphi_N]$ is an $M \times N$ matrix, based on the assumption that M random CS measurements are made. Therefore, if ω represents weights with the smallest N-M ($M \ll N$) coefficients set to zero, the reconstruction of f from y reduces to estimation of the sparse weight vector ω.

A typical method for solving such an ill-posed problem is via the l_p norm of ω:

$$\tilde{\omega} = \arg\min_{\omega}\{\| y - \Phi\omega \|_2^2 + \rho \| \omega \|_p\}, \tag{2}$$

where the scalar ρ ($0 \leqslant p \leqslant 1$) controls the relative importance applied to the Euclidian error and the sparseness term.

Under the common assumption of a zero-mean Gaussian noise, the Gaussian likelihood model can be obtained as

$$p(y \,|\, \omega, \sigma^2) = (2\pi\sigma^2)^{-M/2} \cdot \exp(-\frac{1}{2\sigma^2} \| y - \Phi\omega \|^2). \tag{3}$$

In the above analysis, the CS problem of inverting for the sparse weights ω is converted into a linear-regression

problem with the constraint that ω is sparse. Assuming that Φ is known, quantities that are to be estimated based on the CS measurements y are the sparse weights ω and the noise variance σ^2. In a Bayesian analysis, this is equivalent to seeking a full posterior density function for ω and σ^2.

The l_1 regularization formulation is equivalent to using a Laplace density function prior on the coefficients ω, that is

$$p(\omega\,|\lambda) = \frac{\lambda}{2}\exp(-\lambda\,|\omega|). \qquad (4)$$

Given the CS measurements y, and assuming the likelihood function in Eq. (3), it can be demonstrated in a straightforward manner that the solution in Eq. (2) corresponds to a *maximum a posteriori* (MAP) approximation to a Bayesian linear-regression analysis. However, this formulation of the Laplace prior does not allow for a tractable Bayesian analysis, because it is not a conjugate to the conditional distribution in Eq. (3). To alleviate this issue, RVM has been addressed previously in sparse Bayesian learning. As the first stage of a hierarchical model, the following prior is employed on ω:

$$p(\omega\,|\alpha) = \prod_{i=1}^{N} N(\omega_i\,|0,\alpha_i^{-1}), \qquad (5)$$

where α_i is the precision of a Gaussian density function. Further, a Gamma prior is considered over α:

$$p(\alpha\,|a,b) = \prod_{i=1}^{N} \Gamma(\alpha_i\,|a,b). \qquad (6)$$

By marginalizing over the hyper-parameters α, the overall prior on ω is

$$p(\omega\,|a,b) = \prod_{i=1}^{N} \int_0^{\infty} N(\omega_i\,|0,\alpha_i^{-1})\Gamma(\alpha_i\,|a,b)\mathrm{d}\alpha_i, \qquad (7)$$

where the density function $\Gamma(\alpha_i\,|a,b)$ is the conjugate prior for α_i, ω_i plays the role of observed data, and $N(\omega_i\,|0,\alpha_i^{-1})$ is a likelihood function. Consequently, the integral $\int_0^{\infty} N(\omega_i\,|0,\alpha_i^{-1})\Gamma(\alpha_i\,|a,b)\mathrm{d}\alpha_i$ can be evaluated analytically, and it can be found to correspond to the Student's t-distribution. With appropriate choice of a and b of λ, the Student's t-distribution is strongly peaked around $\omega_i = 0$; therefore, the prior in Eq. (7) favors most ω_i being zero, and the inverse of the noise variance $\alpha_0 = 1/\sigma^2$ is introduced by the Gamma prior.

By combining the stages of the hierarchical Bayesian model, the joint distribution can, finally, be defined as

$$p(\omega,\alpha,\lambda,\sigma^2,y) = p(y\,|\omega,\sigma^2)p(\omega\,|\alpha)p(\alpha\,|a,b)p(a,b). \qquad (8)$$

By Bayes' rule, assuming that the hyper-parameters α and α_0 are known and the measurement value g and the projection matrix Φ are given, then ω can be expressed as a multivariate Gaussian distribution $p(\omega\,|y,\alpha,\sigma^2) \propto N(\mu, \sum)$ with mean and covariance of

$$\mu = \alpha_0 \sum \Phi^{\mathrm{T}} y, \qquad (9)$$

$$\sum = (\alpha_0\Phi^{\mathrm{T}}\Phi + A)^{-1}, \qquad (10)$$

where $A = \mathrm{diag}(\alpha_1,\alpha_2,\cdots,\alpha_N)$. Specifically, by marginalizing over the weights ω, the logarithm $L(\alpha,\alpha_0)$ for α and α_0 can be expressed analytically as

$$L(\alpha,\alpha_0) = \log p(g\,|\alpha,\alpha_0) = \log \int p(g\,|\omega,\alpha_0)p(\omega\,|\alpha)\mathrm{d}\omega$$

$$= -\frac{1}{2}[K\log 2\pi + \log|C| + g^{\mathrm{T}}C^{-1}g], \qquad (11)$$

where $C = \sigma^2 I + \Phi A^{-1}\Phi^{\mathrm{T}}$ (I denotes the orignal image), a type-II maximum likelihood (ML) approximation employs point estimates for α and α_0 to maximize Eq. (11), which can be implemented via the expectation-maximization (EM) algorithm to yield the optimal value.

It is useful to have a measure of uncertainty in the mean and covariance of the weights ω; however, the quantity that draws most interest is the signal $y = \Phi\omega$. ω is drawn from a multivariate Gaussian distribution with mean and covariance defined in Eqs. (8) and (9); therefore, the posterior density function on f is also a multivariate Gaussian distribution with mean and covariance of

$$E(f) = \Psi\mu, \qquad (12)$$

$$\mathrm{Cov}(f) = \Psi \sum \Psi^{\mathrm{T}}. \qquad (13)$$

The diagonal elements of the covariance matrix in Eq. (13) provide "error bars" on the accuracy of the inversion of f, as represented in terms of its mean in Eq. (12).

Natural images can often be compressed with slight or imperceptible loss of information[12]. Most PAT images are sparse in an appropriate transform domain[5]. As a consequence, photoacoustic signals and images can be reconstructed with good accuracy from relatively few measurements by the BCS method.

The BCS method is applied to PAT imaging from an arc mask data acquisition. Figure 1 depicts the diagram of photoacoustic data acquisition in the BCS method with a single transducer. This method requires an optical mask to realize random illumination in data acquisition and utilizes the sparsity of photoacoustic images in the reconstruction. The objective for the use of random illumination is to realize the compression of data along the arc and to reduce the acquisition time. The mask is placed between the laser source and the sample to realize the sparse measurement Φ. It transfers the diversity of measure to realize the exact recovery. To realize the random illumination of the sample, the optical arc mask uses the digital micro-mirror device (DMD), which is modulated according to the Gaussian random matrix by the computer. The mask changes its optical absorption-distribution pattern randomly for each laser light pulse. In addition, the single-element unfocused ultrasonic transducer can record photoacoustic signals for each mask pattern. The Gaussian random matrix is maximally incoherent with any sparsity transform, and therefore, it can be modeled as the random binary Gaussian distribution-measurement matrix to decide whether light passes through the mask.
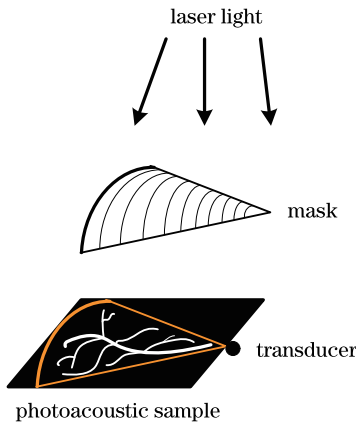
Fig. 1. Data acquisition illustration of the proposed BCS method.

In the course of photoacoustic image reconstruction, the transducer has a limited view via a sector window; therefore, the photoacoustic signals achieved are superpositions of the signal along the arc line. When the sample is fully enclosed in the detection region, accurate recovery is possible from the sparse signal. Further, it requires fewer signals in the near field and more signals in the far field to complete the image reconstruction. Therefore, the matrix Φ can be suitably modified for the scanned photoacoustic sample area. From Fig. 1, it is apparent that the matrix elements outside the sector window can be defined as 0, and the matrix elements inside the sector window can be defined as 0/1, subject to Gaussian distribution. Therefore, the modified matrix Φ_m can not only improve the sparsity and inherence with Ψ, but also lower the mask cost and improve the photoacoustic image quality because of its specific pattern.

The generated acoustic waves along the same arc arrive at the transducer simultaneously, and therefore, signals that are achieved are the information superposition along the arc direction. Thus, photoacoustic signals are collected by a single-element transducer in polar coordinates. Therefore, following BCS reconstruction, these images should undergo the scan conversion; the course for this is presented in Fig. 2, and, if (x, y) is the position of the final photoacoustic image, the conversion to (R, θ) is

$$x = x_0 - R\sin\theta, y = R\cos\theta, \qquad (14)$$

where θ is the deflection angle and (R, θ) is the polar coordinates corresponding to the Cartesian coordinates (x, y).
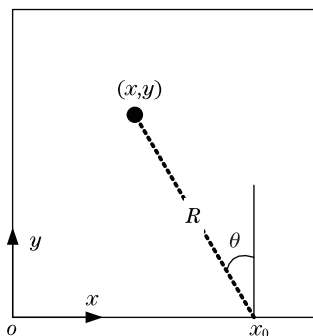

Fig. 2. Schema of scan conversion.

To prove the efficacy and superiority of the BCS method in PAT image reconstruction, photoacoustic signals were simulated by the K-wave Matlab toolbox[13].

In the experiment, the matrix can be implemented by a DMD as a mask. The sample was non-uniformly illuminated realized by the mask. The spatial pattern of the mask can be altered by the digital logical control circuit, which can create the time-varying switch array. The BCS algorithm was used to reconstruct PAT images with a size of 256×256 pixels, as shown in Fig. 3(a). These images were scarified in the discrete wavelet transform (DWT) domain by decomposing them in five scales using the "sym4" wavelet. With the exception of the original image (noiseless), three noisy versions were generated by adding a zero-mean Gaussian noise, and this resulted in signal-to-noise ratios (SNRs) of 5, 10, and 15 dB.

In these experiments, the performance of BCS was compared with the basis pursuit (BP), orthogonal matching pursuit (OMP) and stagewise orthogonal matching pursuit (STOMP) algorithms. The STOMP algorithm was equipped with the constant false discovery rate (CFDR) and the constant false alarm rate (CFAR) thresholding rules. Certain CS methods were applied to the compressive measurements y to reconstruct the PAT image, as shown in Figs. 3(b)–(f).

The quality of the reconstructed image is measured via the reconstruction error, which is defined as follows:

$$E_R = \frac{\| I_{CS} - I \|_2}{\| I \|_2}, \qquad (15)$$

where I and I_{CS} denote the original and reconstructed images and $\| I \|_2$ denotes the two-norm of the image I.

Results depicted in Fig. 3 indicate that the reconstruction of the photoacoustic image from STOMP algorithm represents the worst performance, which cannot obtain the source-image details and has serious artifacts, and this make it an unsuitable algorithm for PAT. Further, the full performance comparisons are summarized in Table 1, and it shows the respective reconstruction error and running time for BP, OMP, and BCS when using
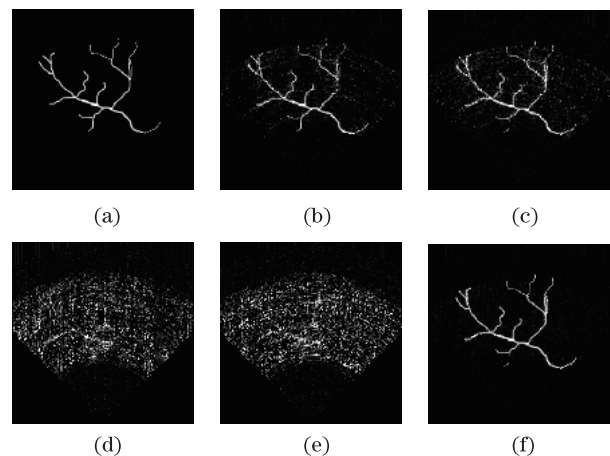

Fig. 3. Reconstruction of photoacoustic image from different CS methods using 100 masks. (a) Original image; (b) reconstruction from BP; (c) reconstruction from OMP; (d) reconstruction from STOMP-CFDR; (e) reconstruction from STOMP-CFAR; (f) reconstruction from BCS.

Table 1. Reconstruction Performances of BP, OMP,
and BCS Methods on PAT Images in Terms of
Reconstruction Error E_{R} and Running Time t

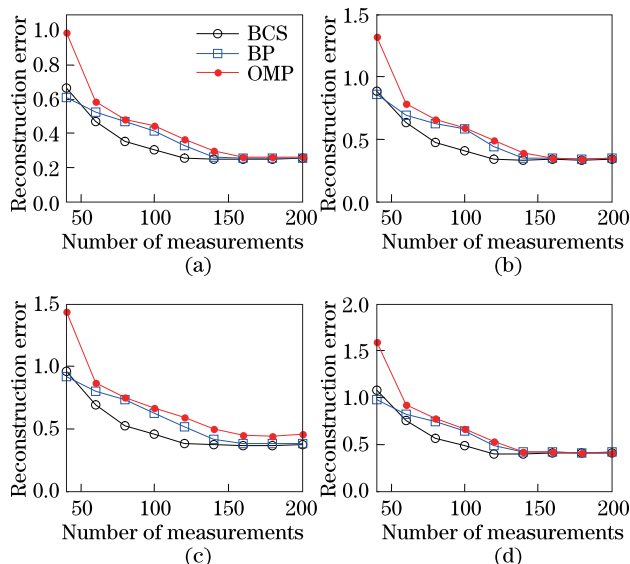| PAT	BP Method		OMP Method		BCS Method	
Images	E_{R}	$t(\mathrm{s})$	E_{R}	$t(\mathrm{s})$	E_{R}	$t(s)$
Noiseless	0.4205	17.4067	0.4446	3.8852	0.3099	10.1153
SNR=15 dB	0.5844	23.5089	0.5869	4.2557	0.4101	14.9492
SNR=10 dB	0.6240	25.1564	0.5899	4.7917	0.4603	16.3291
SNR=5 dB	0.6472	25.3660	0.6631	4.5291	0.4811	17.0752

Fig. 4. Reconstruction errors for different CS algorithms. (a) Noiseless observation; (b) noisy observation with SNR=15 dB; (c) noisy observation with SNR=10 dB; (d) noisy observation with SNR=5 dB.

100 masks. Figure 4 shows the tendency chart of reconstruction errors in reconstructed photoacoustic images obtained from the three CS reconstruction methods under four different conditions. It can be demonstrated that the BCS algorithm has a lesser running time as well as the minimum reconstruction error. Therefore, the BCS method can not only use the fewest measurements to obtain the best performance, but also maintain the best effects irrespective of whether PA signals are noiseless or noisy.

It is notable that the BCS method does not require parameter turning, while the other CS methods require estimation of algorithm parameters from their measurements. In these four sets of experiments, the test was repeated 100 times and the average was expressed by the reconstruction error. It is clear that the BCS method provides the best performance among all the methods tested, and it has the smallest reconstruction error with a minimum number of measurements. Compared with other CS methods, the BCS method provides an estimation of the posterior density function of additive noise in CS measurements and uses the fast RVM algorithm with an objective to achieve highly efficient computations. The fast algorithm maintains a more concise signal representation and the RVM provides a tighter approximation to the l_0-norm sparsity measure than the l_1-norm. It can be proved that, even in the worst-case scenario, the RVM still outperforms the most widely used sparse representation algorithms, including BP, OMP, and STOMP. Therefore, the BCS method provides the best reconstructed image of PAT among all CS methods.

In conclusion, by incorporating the BCS method in PAT image reconstruction, only one single-element unfocused ultrasonic transducer is employed. As a result, the PAT system becomes simpler. In particular, the proposed algorithm can automatically estimate the optimal model parameters from observation data and demonstrates better performance than the other state-of-the-art CS algorithms.

References

1. L. V. Wang, Med. Phys. **35,** 5758 (2008).
2. K. Geng, "Photoacoustic and thermoacoustic tomography: system development for biomedical applications" PhD. Thesis (Texas A&M University, College Station, 2004).
3. L. V. Wang, Disease Markers **19,** 123 (2004).
4. K. Maslov, H. F. Zhang, S. Hu, and L. V. Wang, Opt. Lett. **33,** 929 (2008).
5. X. Yang, X. Cai, K. Maslov, L. Wang, and Q. Luo, Chin. Opt. Lett. **8,** 609 (2010).
6. J. Provost and F. Lesage, IEEE Trans. Med. Imaging **28,** 585 (2009).
7. D. Liang, H. F. Zhang, and L. Ying, Int. J. Function. Inform. Personal. Med. **2,** 394 (2009).
8. Z. Guo, C. Li, L. Song, and L. V. Wang, J. Biomed. Opt. **15,** 021311 (2010).
9. Z. Ren, G. Liu, Z. Huang, W. Zeng, and D. Li, Proc. SPIE **7382,** 73822R (2009).
10. J. Feng, K. Jia, C. Qin, S. Zhu, X. Yang, and J. Tian, Chin. Opt. Lett. **8,** 1010 (2010).
11. S. Ji, Y. Xue, and L. Carin, IEEE Trans. Signal Process. **56,** 2346 (2008).
12. M. G. Strintzis, Int. J. Med. Inform. **52,** 159 (1998).
13. B. E. Treeby and B. T. Cox, J. Biomed. Opt. **15,** 021314 (2010).